Characterization of Microstrip Discontinuities on Multilayer Dielectric Substrates Including Radiation Losses

WILLIAM P. HAROKOPUS, JR., MEMBER, IEEE, AND PISTI B. KATEHI, SENIOR MEMBER, IEEE

Abstract—**A two-dimensional space-domain method of moments treatment of open microstrip discontinuities on multi-dielectric-layer substrates is presented. The full-wave analysis accounts for electromagnetic coupling, radiation, and all substrate effects. The technique has been utilized to characterize commonly used discontinuities on one and two dielectric layers, and numerical results for step, corner, and T-junction discontinuities are included.**

I. INTRODUCTION

MONOLITHIC circuit applications continue to extend farther into the millimeter-wave range, approaching terahertz frequencies. At these frequencies, planar transmission line structures are required for passive component design. In particular, microstrip components are frequently utilized in MMIC circuit applications. Unfortunately, available microstrip CAD discontinuity and circuit element models fail to account for electromagnetic effects, which become significant with increasing frequency. Without reliable CAD, microwave design engineers will face unacceptably lengthy development cycles.

The preponderance of the available microstrip CAD is based on quasi-static methods [1]–[6], equivalent waveguide models [7]–[10], and semiempirical models [11]. These models require little computational effort, but fail to adequately account for electromagnetic coupling, radiation, and surface wave excitation. Quasi-static methods provide accurate characterization only at lower frequencies, while planar waveguide models contain limited information on dispersion.

Consequently, an analysis accounting for electromagnetic coupling, space wave, and surface wave radiation is required for the characterization of microstrip discontinuities, couplers, and matching elements at higher frequencies. Increasingly powerful computers and innovative techniques make full electromagnetic analysis a realistic alternative in the design of high-frequency microstrip circuits. Full-wave analysis has already demonstrated accuracy in modeling simple microstrip discontinuities on single dielectric layers.

Often, microstrip discontinuities and elements are enclosed in a package or a cavity. Jansen has performed an analysis of irregular covered microstrip elements with a spectral-domain technique [12]. Shielded microstrip discontinuities such as open ends, gaps, stubs [13], and coupled line filters [14] have been studied by the method of moments.

Nonetheless, microstrip is often used in the design of feeding networks for monolithic antenna arrays. Unlike shielded microstrip, open microstrip discontinuities are free to radiate. Also, the microstrip substrate supports surface wave modes. High-frequency microstrip design requires a thorough understanding of these effects. Full electromagnetic solutions have been performed on open microstrip elements which are electrically thin, such as open ends, gaps, and coupled lines [17]–[19]. These solutions are based on the thin strip approximation, and utilize one-dimensional method of moments. Under this assumption, the transverse current component gives a second-order effect and may be neglected. In addition, an analysis of open-end and gap discontinuities in a substrate–superstrate configuration has been performed [20]. More recently, spectral-domain solution was applied to irregular step and stub elements on a single layer [21]. However, the characterization of these microstrip elements is far from complete. The fact that these elements are parts of antenna feeding networks necessitates a serious consideration of the coupling and radiation losses and their effect on the performance of the antenna. In addition, in monolithic arrays, multiple dielectric layers offer many advantages in designing feeding networks: they allow alternative solutions to circuit layouts or can provide protection in the form of superstrates. Furthermore, the appropriate combination of dielectric and semiconducting materials can create circuits with desirable properties such as slow-wave structures. This paper addresses, for the first time, the problem of accurate characterization of microstrip discontinuities on multilayer substrates and carefully studies the effects of this dielectric structure on circuit performance.

The presented full-wave analysis is based on the application of two-dimensional method of moments in the space

Manuscript received March 31, 1989; revised July 24, 1989. This work was supported by the National Science Foundation under Grant ECS-8602536 and by the Army Research Office under Contract DAALO3-k-0088 (23836-EL).

The authors are with the Radiation Laboratory, Electrical Engineering and Computer Science Department, 1301 Beal Ave., University of Michigan, Ann Arbor, MI 48109.

IEEE Log Number 8931087.

0018-9480/89/1200-2058$01.00 ©1989 IEEE

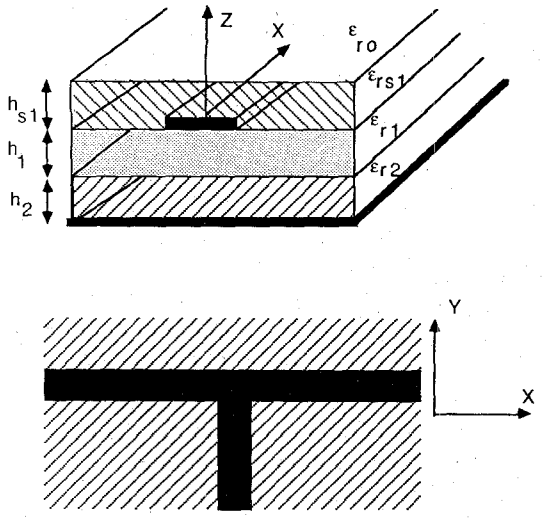

Fig. 1. Multilayer open microstrip geometry.

domain. The dyadic Green's function for a grounded multi-dielectric-layer configuration is employed to develop an algorithm capable of analyzing structures with an arbitrary number of layers. Included in the solution are both transverse and longitudinal current components, allowing the treatment of a wide class of irregular microstrip elements including steps of width, corners, and T junctions. On the microstrip conductors, both current components are expanded by rooftop basis functions. Once the current distribution is evaluated, transmission line theory is employed to determine the network parameters.

Numerical results from this technique have demonstrated excellent agreement with measurement and the spectral-domain technique in the case of single dielectric layers. Scattering parameters will be presented for corner and for T-junction discontinuities on one layer and on more complicated dielectric structures. In addition, on a single layer the more complex geometry of a meander line containing four coupled bends will be presented. The implemented method fully accounts for coupling, space, and surface wave radiation and for all dispersive effects.

II. Analysis

Much of the published work on full-wave analysis of open microstrip discontinuities has been limited to structures with strip widths much smaller than the microstrip wavelength ($w \ll \lambda_g$). Under this approximation, the transverse current component can be considered a second-order effect and neglected [16]. Therefore, analysis was restricted to thin-strip discontinuities such as open ends, gaps, and coupled line filters. Obviously, the transverse current component is critical for the analysis of irregular structures such as steps in width, corners, and T junctions, and is therefore included in this analysis.

The general multilayer open microstrip geometry is shown in Fig. 1. The dielectric layers are considered lossless, but the development is not limited by this assumption. The conductors have infinite conductivity, with the strip conductor being of finite thickness ($t \ll \lambda_g$). Maxwell's equations and the application of Green's identities yield Pocklington's integral equation for the electric field:

$$\vec{E}(\vec{r}) = \int\int_{S'} \overline{\overline{G}}(\vec{r}, \vec{r}') \cdot \vec{J}(x', y')\, dx'\, dy' \tag{1}$$

where $\vec{E}(\boldsymbol{r})$ is the total electric field at the point $\boldsymbol{r} = (x, y, z)$, $\vec{J}(x', y')$ is the unknown current on the microstrip conducting strip, and $\overline{\overline{G}}(\vec{r}, \vec{r}')$ is the dyadic Green's function for x- and y-directed Hertzian dipoles above a grounded multilayer slab.

To provide for the most general solution possible, strip conductors may be located on any interface. A general, numerically efficient Green's function for an arbitrary number of layers may be derived by decomposing the fields into LSE and LSM modes with respect to $\hat{z}$ [23]. Cylindrical symmetry may also be exploited by using a Hankel transform in the transverse direction. This results in the one-dimensional boundary value problem, which may be simplified to a two-layer structure by using equivalent impedance boundaries as illustrated in Fig. 2(a). In Fig. 2(b), the equivalent transmission line model for this structure is shown, from which the impedance boundaries can be determined.

After application of the inverse Hankel transform, the solution to the resulting boundary value problem is a compact, computationally efficient space-domain Green's function. For a multilayer geometry with the strip conductor located on the top layer (at the dielectric–air interface) the components of the Green's function are given by

$$G_{xx} = G_{yy} = \frac{\omega\mu_0}{2\pi}\int_0^\infty \lambda J_0(\lambda\rho)\frac{e^{-ju_0 z}}{f_1(\lambda, \epsilon_{r_1}, h_1, \epsilon r_2, h_2, \cdots)}\, d\lambda$$
$$- \frac{1}{2\pi}\frac{d^2}{dx^2}\int_0^\infty \frac{J_0(\lambda\rho)}{\lambda} e^{-ju_0 z}$$
$$\cdot\left[\frac{u_0 u_1}{\omega\epsilon_0}\frac{1}{f_2(\lambda, \epsilon_{r_1}, h_1, \epsilon_{r_2}, h_2, \cdots)}\right.$$
$$\left. - \frac{\omega\mu_0}{f_1(\lambda, \epsilon_{r_1}, h_1, \epsilon_{r_2}, h_2, \cdots)}\right] d\lambda \tag{2}$$

$$G_{xy} = G_{yx} = -\frac{1}{2\pi}\frac{d^2}{dx\,dy}\int_0^\infty \frac{J_0(\lambda_\rho)}{\lambda} e^{-ju_0 z}$$
$$\cdot\left[\frac{u_0 u_1}{\omega\epsilon_0}\frac{1}{f_2(\lambda, \epsilon_{r_1}, h_1, \epsilon_{r_2}, h_2, \cdots)}\right.$$
$$\left. - \frac{\omega\mu_0}{f_1(\lambda, \epsilon_{r_1}, h_1, \epsilon_{r_2}, h_2, \cdots)}\right] d\lambda \tag{3}$$

with $\rho = \sqrt{(x-x')^2 + (y-y')^2}$. In (2) and (3) the semi-infinite integration is over the spectrum of spatial frequencies $\lambda(\lambda^2 = k_x^2 + k_y^2)$, and the parameters $u_n (n = 0, 1, \cdots)$

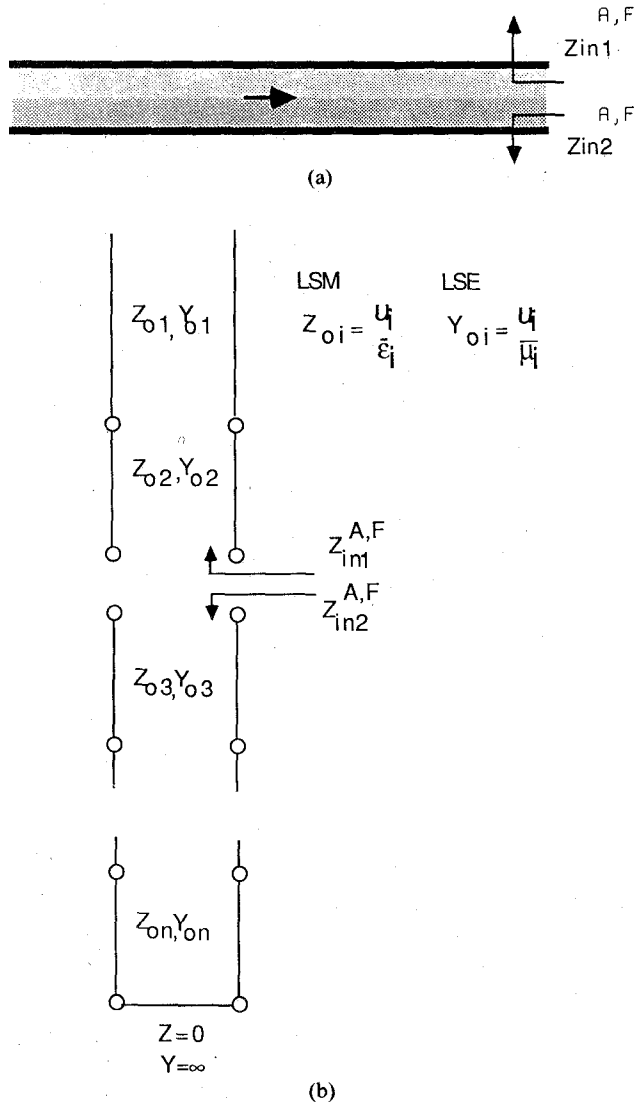

Fig. 2. Derivation of general multilayer Green's function (a) Equivalent impedance boundaries. (b) Transmission line analogue.

are given in terms of λ by the following relation:

$$u_n = \sqrt{k_n^2 - \lambda^2} \tag{4}$$

where k_n is the wavenumber in the nth layer. In addition, in (2) and (3) the functions $f_1(\lambda, \epsilon_{r1}, h_1, \cdots)$ and $f_2(\lambda, \epsilon_{r1}, h1, \cdots)$ are the characteristic equations for the TE and TM surface wave modes, respectively, and have the form

$$f_1(\lambda, \epsilon_{r1}, h_1, \cdots) = u_0 + u_1 \frac{(1-\Gamma_{f2})}{1+\Gamma_{f2}} \tag{5}$$

$$f_2(\lambda, \epsilon_{r1}, h1, \cdots) = u_1 + \epsilon_{r1} u_0 \frac{(1+\Gamma_{a2})}{(1-\Gamma_{a2})} \tag{6}$$

where Γ_{a2} and Γ_{f2} are the reflection coefficients looking into the substrate, as shown in Fig. 2(b). The surface wave characteristic equations contain all of the information for the dielectric layers not adjacent to the current source within the parameters $\Gamma_{a,f}$. For the case of a single layer, the solution simplifies to the space-domain Sommerfeld Green's function [24], [25]:

$$G_{xx} = G_{yy} = \frac{\omega\mu_0}{2\pi}\int_0^\infty \lambda J_0(\lambda\rho)\frac{e^{-ju_0 z}}{f_1(\lambda, \epsilon_{r1}, h_1)} - \frac{1}{2\pi}\int_0^\infty \frac{d^2}{dx^2} e^{-ju_0 z}\frac{J_0(\lambda\rho)}{\lambda} \cdot \left[\frac{u_0 u_1}{\omega\epsilon_0}\frac{1}{f_2(\lambda, \epsilon_{r1}, h_1)} - \frac{\omega\mu_0}{f_1(\lambda, \epsilon_{r1}, h_1)}\right] d\lambda \tag{7}$$

$$G_{xy} = G_{yx} = -\frac{1}{2\pi}\int_0^\infty \frac{d^2}{dx\,dy} e^{-ju_0 z}\frac{J_0(\lambda\rho)}{\lambda} \cdot \left[\frac{u_0 u_1}{\omega\epsilon_0}\frac{1}{f_2(\lambda, \epsilon_{r_1}, h_1)} - \frac{\omega\mu_0}{f_1(\lambda, \epsilon_{r_1}, h_1)}\right] d\lambda \tag{8}$$

where

$$f_1(\lambda, \epsilon_{r1}, h_1) = u_0 + u_1 \coth ju_1 h_1 \tag{9}$$

$$f_2(\lambda, \epsilon_{r1}, h_1) = \epsilon_r u_0 + u_1 \tanh ju_1 h_1. \tag{10}$$

In the above, ϵ_{r1} is the relative dielectric constant, and h_1 is the thickness of the substrate.

The method of moments [26] is applied to transform Pocklington's integral equation to a system of linear equations. The microstrip discontinuity is subdivided into overlapping squares. The transverse and longitudinal current components on the microstrip are expanded over these squares by finite series

$$J_x = \sum_{n=1}^{N+1}\sum_{m=1}^{M+1} I_{nm}^x j_{nm}^x(x', y') \tag{11}$$

$$J_y = \sum_{n=1}^{N+1}\sum_{m=1}^{M+1} I_{nm}^y j_{nm}^y(x', y') \tag{12}$$

where

$$j_{n,m}^x(x', y') = [f_n(x') g_m(y')] \tag{13}$$

$$j_{n,m}^y(x', y') = [g_n(x') f_m(y')]. \tag{14}$$

In (11) and (12), I_{nm} is the unknown current amplitude at the (n, m)th position of the subdivided element. The functions f_n and g_m are subdomain shaping or basis functions and are consistent with the current boundary conditions. The subdomain basis functions have piecewise-sinusoidal variation in the longitudinal direction and constant variation in the transverse direction according to

$$f_n(x') = \begin{cases} \dfrac{\sin k(x_{n+1} - x')}{\sin kl_x}, & x_n \leqslant x' \leqslant x_{n+1} \\ \dfrac{\sin k(x' - x_{n-1})}{\sin kl_x}, & x_{n-1} \leqslant x' \leqslant x_n \\ 0, & \text{else} \end{cases} \tag{15}$$

and

$$g_m(y') = \begin{cases} 1, & y_{m-1} \leqslant y' \leqslant y_{m+1} \\ 0, & \text{else.} \end{cases} \tag{16}$$

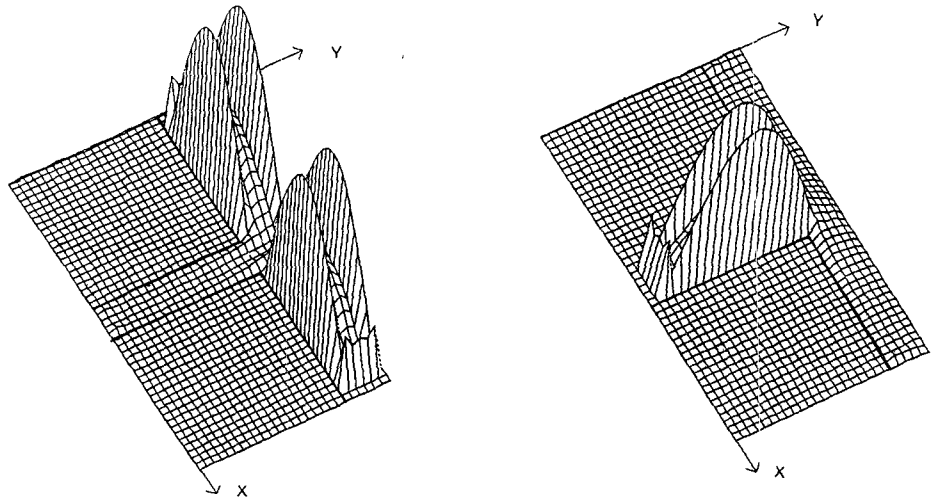

Fig. 3. Current on T junction excited by gap generators ($\epsilon_r = 4$, $h = 0.4$ mm, $W = 0.2$ mm). (a) Current component $J_x(x, y)$. (b) Current component $J_y(x, y)$.

In the above, $l_x = x_{n+1} - x_n$, and k is a scaling parameter chosen to vary between k_0 (free-space wavenumber) and k (wavenumber in the dielectric). The numerical solution has shown that best stability occurs when the scaling constant is chosen close to the guide wavelength. Substitution of the above into Pocklington's integral equation (1) yields a system of linear equations in the form

$$E_x + \Delta E_x = \sum_{n=1}^{N+1} \sum_{m=1}^{M+1} Z_{xx}^{nm} I_x^{nm} + Z_{xy}^{nm} I_y^{nm} \tag{17}$$

$$E_y + \Delta E_y = \sum_{n=1}^{N+1} \sum_{m=1}^{M+1} Z_{yx}^{nm} I_x^{nm} + Z_{yy}^{nm} I_y^{nm} \tag{18}$$

where $Z_{ij}^{nm}(i, j = x, y)$ constitutes the contribution of the jth component of current to the ith component of the electric field from the current element on the (nm)th subdivision. The terms ΔE_x and ΔE_y represent the errors in the electric field due to the approximations made in the current.

During the derivation of the Green's function, all applicable boundary conditions for the grounded multidielectric geometry were applied, with the exception of the condition on the microstrip conductors. This condition, which states that the tangential electric field has to go to zero on the surface of the conducting strips, will be enforced through the method of moments procedure. In addition, it has been shown that Galerkin's procedure represents a strong condition on the minimization of the errors ΔE_x and ΔE_y. For this procedure, the following inner products are defined:

$$V_{\nu\mu}^x = \langle j_{\nu\mu}(\vec{r}), E_x \rangle = \int_{x_{n-1}}^{x_{n+1}} \int_{y_{m-1}}^{y_{m+1}} (E_x + \Delta E_x) f_\nu(x) g_\mu(y)\, dx\, dy \tag{19}$$

$$V_{\nu\mu}^y = \langle j_{\nu\mu}(\vec{r}), E_y \rangle = \int_{x_{n-1}}^{x_{n+1}} \int_{y_{m-1}}^{y_{m+1}} (E_y + \Delta E_y) f_\nu(y) g_\mu(x)\, dx\, dy \tag{20}$$

where $f_\nu(x)$ and $g_\mu(y)$ are testing functions identical to the basis functions and $\nu = 1, \cdots, N+1$, and $\mu = 1, \cdots, M+1$. In view of (19) and (20), equations (17) and (18) result in the following matrix equation:

$$\begin{bmatrix} ZXX_{nm}^{\nu\mu} & ZXY_{nm}^{\nu\mu} \\ ZYX_{nm}^{\nu\mu} & ZYY_{nm}^{\nu\mu} \end{bmatrix} \begin{bmatrix} I_x^{nm} \\ I_y^{nm} \end{bmatrix} = \begin{bmatrix} V_{\nu\mu}^x \\ V_{\nu\mu}^y \end{bmatrix}$$

where $ZIJ_{nm}^{\nu\mu}(I, J = X, Y)$ represent blocks of the impedance matrix, I_i is the vector of unknown x and y current amplitudes, and V_j is the excitation vector which is identically zero everywhere except at the position of the source. Once the matrix inversion is performed, the current amplitudes on the feeding lines are known.

In order to extract the scattering parameters, the discontinuity is excited systematically at all ports by delta gap generators. Assuming a unimodal field excited on the microstrip feeding line, beyond a reference plane the current forms TEM-like standing waves. Transmission line theory can then be used to extract the scattering parameters for a network from the standing wave patterns on the feeding lines. The presence of the gap is reflected in the excitation vector, where

$$V_x^{\nu\mu} = \begin{cases} 1 & \text{if } x_\nu = x_g \\ 0 & \text{else} \end{cases} \tag{21}$$

and

$$V_y^{\nu\mu} = \begin{cases} 1 & \text{if } y_\mu = y_g \\ 0 & \text{else} \end{cases}. \tag{22}$$

In the above, x_g and y_g are positions of an x-oriented and a y-oriented gap generator respectively.

In Fig. 3, the three-dimensional plot depicts the current on a T junction excited at all three of its ports by gap generators. As illustrated, the current assumes a uniform standing wave pattern along the feeding lines of the discontinuity. With a length of feed line longer than that shown, the current SWR and the positions of minima can be determined. The considered minima are away from the discontinuity, far enough for higher order modes to have

vanished. The reflection coefficient at a reference plane $X = L$ looking in any port is

$$\Gamma(L) = \frac{SWR - 1}{SWR + 1} e^{j - 4\pi(L - X_{\min})/\lambda_g} \tag{23}$$

where SWR is the current standing wave ratio, and $X_{\min}$ is the position of a current minimum. The microstrip guide wavelength λ_g has been previously determined from a long open-ended line.

From the reflection coefficient, the normalized input impedance may be determined according to

$$Z_{\text{in}} = \frac{1 + \Gamma(L)}{1 - \Gamma(L)}. \tag{24}$$

To evaluate the network parameters, an N-port discontinuiy must be excited by N independent excitations. In the case of a symmetrical two-port, even and odd excitations may be employed. For the even case the gap generators are of equal magnitude and phase, and for the odd case they have equal magnitude and are out of phase by 180°. The even and odd input impedances, obtained from (23) and (24), may be combined to give the elements for the Z matrix, which for the case of a symmetric network take the form

$$Z_{11} = \frac{Z_{\text{in}}^{1e} + Z_{\text{in}}^{1o}}{2} \tag{25}$$

$$Z_{22} = Z_{11} \tag{26}$$

$$Z_{12} = \frac{Z_{\text{in}}^{1o} - Z_{\text{in}}^{1e}}{2} \tag{27}$$

$$Z_{12} = Z_{21}. \tag{28}$$

In the above, $Z_{\text{in}}^{1e(o)}$ refers to port 1 under an even (odd) excitation. For nonsymmetric networks and multiport networks similar expressions may be obtained. The scattering parameters are obtained from the Z matrix by a simple transformation.

Finally, the total radiation losses may be determined from the known relation

$$\frac{P_{\text{rad}}}{P_{\text{in}}} = 1 - |S_{11}|^2 - |S_{12}|^2. \tag{29}$$

III. Evaluation of Impedance Matrix Elements

The numerical evaluation of the Sommerfield integrations involved in the Green's function is quite involved. A detailed discussion of the evaluation of the Sommerfeld integrations has been included in a previous work [29] by one of the authors and will not be discussed further here.

In the matrix equation of Section II, the terms $ZXX_{nm}^{\nu\mu}$ and $ZYY_{nm}^{\nu\mu}$ represent the interactions between the x or y components located in the (n, m)th and (ν, μ)th cells. The terms $ZXY_{nm}^{\nu\mu}$ and $ZYX_{nm}^{\nu\mu}$ represent the interaction between the x and y components located in the (n, m)th and (ν, μ)th cells. The computation of all of the 2 $(NM)^2$ interactions would be extremely time consuming. Yet, the number of computations can be greatly reduced noting the following points. For the directly coupled blocks, due to the symmetry and the even valueness of the Green's function with respect to the x and y separations, all interactions between subsections depend only on the magnitudes $|x - x'|$ and $|y - y'|$. For the cross-coupled blocks, the symmetry and the odd valueness of the Green's functions may lead to similar conclusions. Thus, vectors of impedance matrix elements may be precomputed and catalogued according to separations for various substrates and subsection sizes. These libraries can then be used repeatedly for discontinuity analysis.

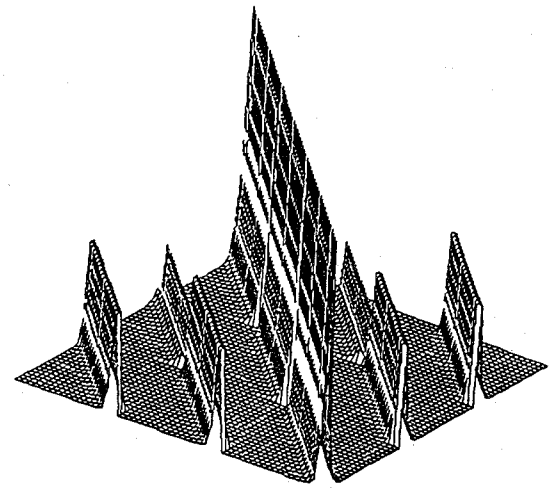

Fig. 4. Toplitz impedance matrix.

A typical impedance matrix is plotted in Fig. 4. As illustrated, the matrix is Toplitz, with the diagonal elements being the largest by an order of magnitude. Although not done in the following results, it appears evident from the figure that interactions of subsections electrically distant may be ignored. This could result in further savings in computer time.

IV. Numerical Results

A. Single-Layer Discontinuities

The presented technique has been applied to characterize the discontinuity shown in Fig. 5(a). This matching section is printed on a 10 mil substrate of relative permittivity 9.9. Over the frequency range of interest, the microstrip section and the substrate thickness are electrically small ($< \frac{1}{10}\lambda_g$). As expected, our moment method algorithm has found radiation losses insignificant for this example. Fig. 5(a) and (b) shows the magnitude and phase of the scattering parameters as compared to measurement. As illustrated, the agreement with measurements for magnitude and phase is excellent. In particular, the agreement of the phase is within 2.5° across this frequency range. The measurements were performed by TI using a cascade prober and an 8510 automatic network analyzer.

1) Radiation Losses: Radiation losses for open microstrip elements can be significant at millimeter-wave frequencies. To illustrate the ability of the analysis presented here to account for space and surface wave losses, a

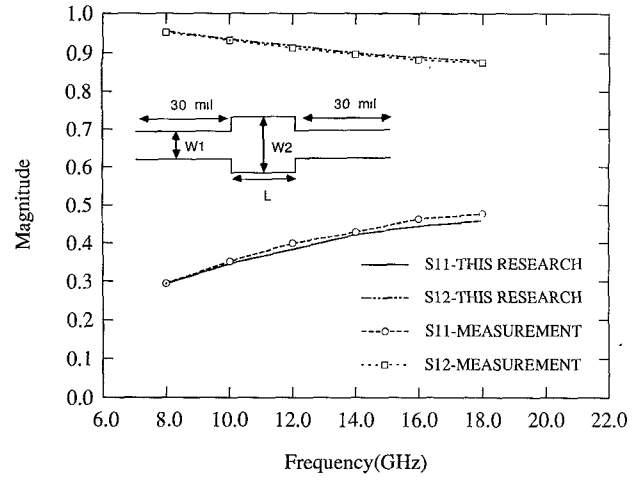

(a)

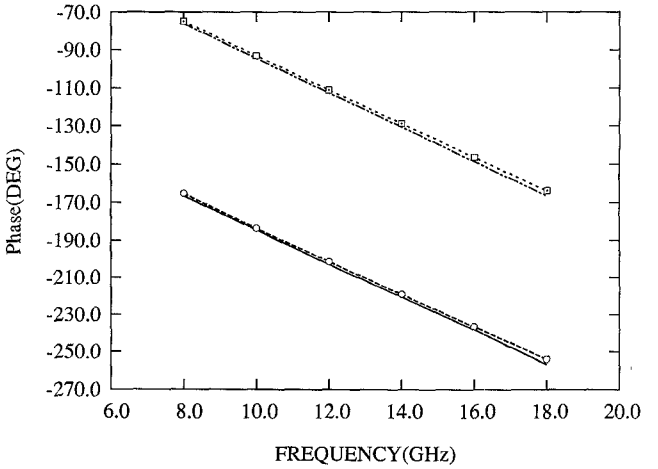

(b)

Fig. 5. Scattering parameters of matching section. Numerical (experimental) dimensions: $W1 = 9.2$ (9.2) mm, $W2 = 23$ (23.1) mm, $L = 50.6$ (50.0), $\epsilon_r = 9.9$, $h = 10$ mil. (a) Magnitude. (b) Phase.

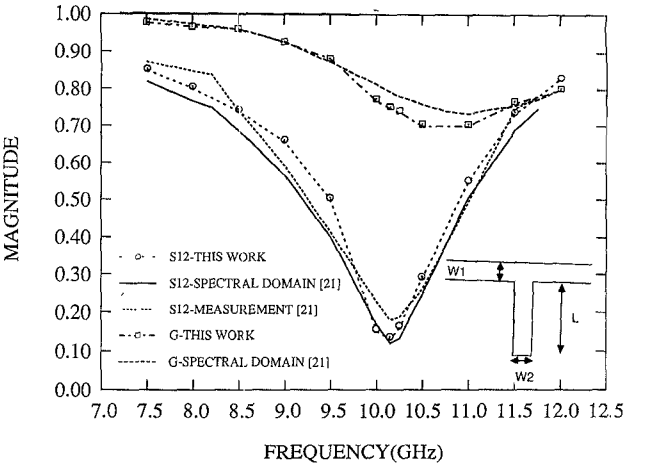

Fig. 6. Scattering Parameters for Microstrip Stub. Space (spectral) dimensions: $W1 = 1.44$ (1.40), $W2 = 1.44$ (1.40), $L = 2.16$ (2.16), $\epsilon_r = 10.65$, $h = 1.27$ mm.

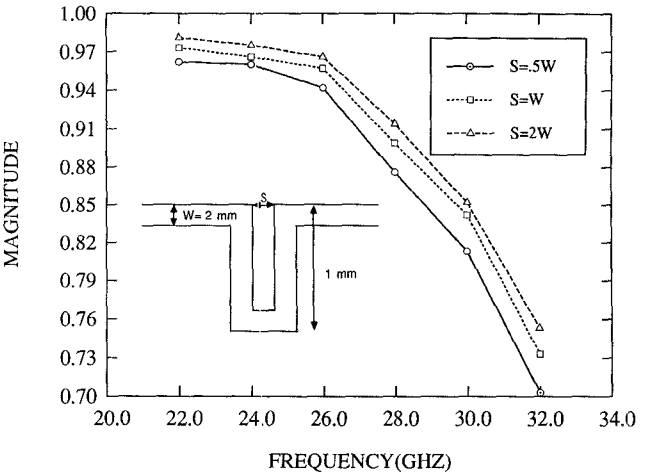

Fig. 7. Design curve for meander line ($\epsilon_r = 9.9$, $h = 10$ mil).

microstrip stub on a single microstrip layer was compared to previously published data obtained with the spectral-domain technique [21]. The microstrip stub contains a T-junction discontinuity and an open end and is printed on a 1.27 mm substrate of dielectric constant 10.65. As illustrated in Fig. 6, the agreement between our space-domain technique and the spectral-domain technique is very good. The quantity denoted G in the graph corresponds to $|S_{11}|^2 + |S_{12}|^2$, which may be subtracted from 1 to determine the total radiated power. The quarter-wave resonance occurs just beyond 10 GHz. Also included in the plot are measurements obtained by Jackson [21].

2) Single-Loop Meander Line: Multiloop meander lines are frequently used in such MMIC's as traveling wave amplifiers for their slow-wave properties. The formulation presented in this paper has been applied to simulate a single-loop meander line in order to illustrate the versatility of the method in modeling irregular microstrip discontinuities. Furthermore, the consideration of a single-loop instead of a multiloop line speeds up the computation and reveals very explicitly the effect of distributed discontinuities and electromagnetic coupling on the slow-wave properties of the structure.

The line is printed on a 10 mil alumina substrate ($\epsilon_r = 9.9$). The magnitude of S_{21} is shown in Fig. 7 as a function of frequency for three values of the width-to-spacing ratio (w/s). In addition, Fig. 8 shows the normalized phase velocity around the loop (v'/v) as a function of frequency, where v is the phase velocity on a microstrip line of length equal to the mean path length of the loop. These results indicate, in this frequency range, that the parasitics in the loop increase the phase velocity v', which in turn tends to reduce the overall slow-wave effect of the meander line.

B. Multilayer Microstrip Discontinuities

A powerful advantage of the presented formulation is its ability to model multilayer substrates by replacing the single-layer Green's function with the multilayer function. The full-wave procedure was applied to a microstrip corner discontinuity on a substrate having two dielectric layers. The magnitudes of the scattering parameters are shown in Fig. 9. The multilayer corner has been analyzed on four different substates: A) a 40 mil layer of alumina

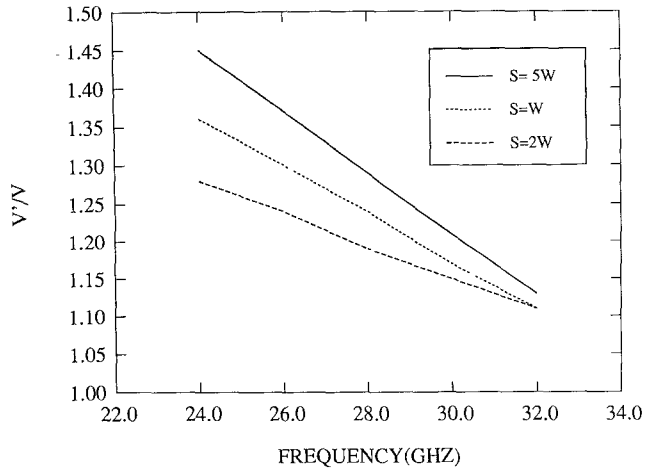

Fig. 8. Phase velocity in meander line.

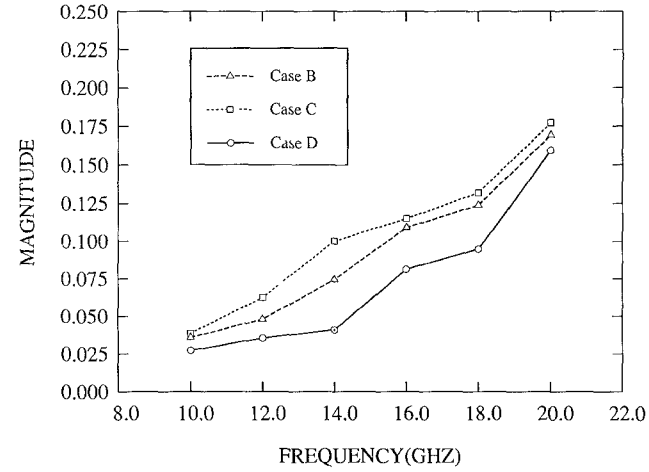

Fig. 10. Radiation from multilayer microstrip corner. $W1 = W2 = 20$ mil.

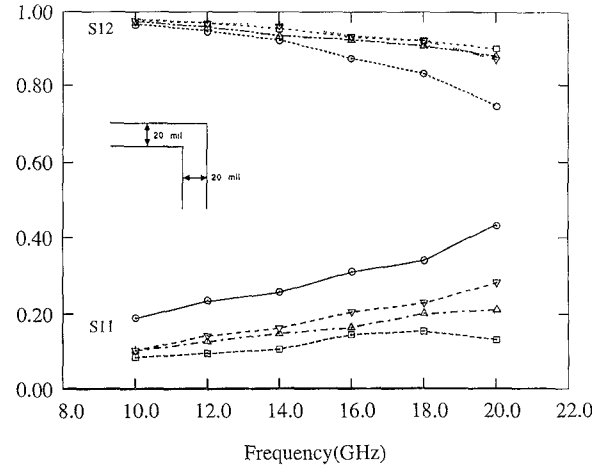

Case	ϵ_{r1}	ϵ_{r2}	$h_1(mil)$	$h_2(mil)$
A	10.2		40	0
B	2.2		40	0
C	2.2	10.2	20	20
D	10.2	2.2	20	20

Fig. 9. Scattering parameters for multilayer microstrip corner. $W1 = W2 = 20$ mil.

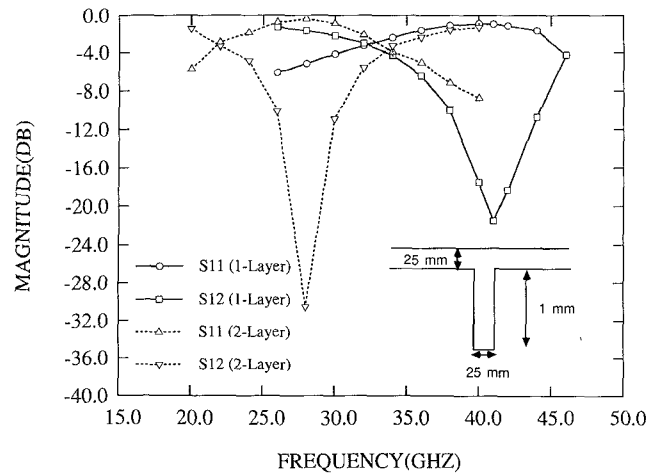

Fig. 11. Scattering parameters for multilayer microstrip stub. $W1 = W2 = 0.2$ mm, $L = 0.6$ mm.

($\epsilon_r = 10.2$); B) a 40 mil layer of Duroid ($\epsilon_r = 2.2$); C) a 20 mil layer of Duroid on a 20 mil layer of alumina; and D) a 20 mil layer of alumina on a 20 mil layer of Duroid.

There is significant difference in radiation between the two multilayer cases. The radiation from the structure having Duroid over alumina is considerably greater than the structure having alumina over Duroid, as illustrated in Fig. 10. It is believed that for this structure the loss is due primarily to surface wave radiation. Therefore, case D couples less power into surface waves than case C. This phenomenon is believed to be related to the suppression of surface wave excitation reported by Jackson [27] in his study of antenna elements.

A two-layer microstrip stub was also analyzed. Shown in Fig. 11 are the magnitudes of the scattering parameters for a stub on substrate having a layer of GaAs ($\epsilon_r = 12.2$) on quartz ($\epsilon_r = 4.0$). Both layers are 0.2 mm thick. Also included are the scattering parameters for a stub having the same dimensions on a single layer of quartz. The single-layer example has a resonant frequency at 41 GHz. The higher effective dielectric constant for the two-layer case creates a stub having a smaller resonant length, and results in a downward shift in frequency for the null of $|S12|$. The radiation losses for both stubs are included in Fig. 12. As illustrated, the multilayer stub shows a tendency to radiate less. This indicates that multilayer substrates may be utilized to reduce radiation losses.

V. Conclusion

A versatile analysis of microstrip discontinuities has been presented. The two dimensional method of moments technique has demonstrated excellent agreement with measurements and other theoretical data derived for a single layer. A powerful extension of the method allows the treatment of discontinuities on more complicated dielectric structures. This is accomplished by employing the Green's function for a conductor-backed multidielectric layer, resulting in the ability to model with full electromagnetic

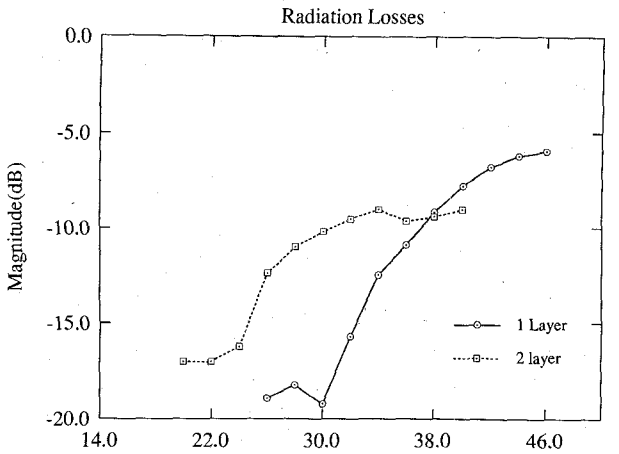

Fig. 12. Radiation from multilayer microstrip stub. $W1 = W2 = 0.2$ mm, $L = 0.6$ mm.

analysis a wide variety of nonuniform microstrip configurations.

Numerical results for corner and T-junction discontinuities have been presented on two dielectric layers. Additionally, the ability of the formulation to model larger elements composed of these building blocks has been demonstrated by the inclusion of a design curve for a meander line.

The full-wave technique accurately accounts for coupling, space wave, and surface wave radiation. Curves of radiation losses are presented for the corner and stub elements.

ACKNOWLEDGMENT

The authors wish to express their gratitude to Dr. S. R. Nelson and A. Crane of Texas Instruments for their contributions to this work.

REFERENCES

[1] M. Maeda, "Analysis of gap in microstrip transmission lines," *IEEE Trans. Microwave Theory Tech.*, vol. MTT-20, pp. 390–396, June 1972.

[2] P. Benedek and P. Silvester, "Equivalent capacitance of microstrip gaps and steps," *IEEE Trans. Microwave Theory Tech.*, vol. MTT-20, pp. 729–733, Nov. 1972.

[3] P. Silvester and P. Benedek, "Equivalent capacitance of microstrip open circuits," *IEEE Trans. Microwave Theory Tech.*, vol. MTT-20, pp. 511–516, Aug. 1972.

[4] P. Silvester and P. Benedek, "Equivalent discontinuities capacitances for right-angle bends, T-junctions, and crossings," *IEEE Trans. Microwave Theory Tech.*, vol. MTT-21, pp. 341–346, May 1973.

[5] R. Horton, "The electrical characterization of right-angle bends in microstrip line," *IEEED Trans. Microwave Theory Tech.*, vol. MTT-21, pp. 427–429, June 1973.

[6] C. Gupta, and A. Gopinath, "Equivalent circuit capacitance for microstrip change in width," *IEEE Trans. Microwave Theory Tech.*, vol. MTT-25, pp. 819–821, Oct. 1977.

[7] T. Itoh, "Analysis of microstrip resonators," *IEEE Trans. Microwave Theory Tech.*, vol. MTT-22, pp. 946–952, Nov. 1974.

[8] I. Wolf, G. Kompa, and R. Mehran, "Calculation method for microstrip discontinuities and T-junctions," *Electron. Lett.*, vol. 8, 1972.

[9] G. Kompa and R. Mehran, "Planar waveguide model for calculating microstrip components," *Electron. Lett.*, vol. 11, 1975.

[10] W. Menzel and I. Wolf, "A method for calculating the frequency dependent properties of microstrip discontinuities," *IEEE Trans. Microwave Theory Tech.*, vol. MTT-25, pp. 107–112, Feb. 1977.

[11] M. Kirschning, R. H. Jansen, and H. L. Koster, "Measurement and computer-aided modeling of microstrip discontinuities by an improved resonator method," in *IEEE MTT-S Int. Microwave Symp. Dig.*, May 1983.

[12] R. H. Jansen, "The spectral domain approach for microwave integrated circuits," *IEEE Trans. Microwave Theory Tech.*, vol. MTT-33, pp. 1043–1056, Oct. 1985.

[13] J. C. Rautio and R. F. Harrington, "An electromagnetic timeharmonic analysis of shielded microstrip circuits," *IEEE Trans. Microwave Theory Tech.*, vol. MTT-35, pp. 726–730, Aug. 1987.

[14] L. P. Dunleavy and P. B. Katehi, "A generalized method for analyzing shielded thin microstrip discontinuities," *IEEE Trans. Microwave Theory Tech.*, vol. 36, pp. 1758–1766, Dec. 1988.

[15] L. P. Dunleavy and P. B. Katehi, "Shielding effects in microstrip discontinuities," *IEEE Trans. Microwave Theory Tech.*, vol. 36, pp. 1767–1774, Dec. 1988.

[16] P. B. Katehi and N. G. Alexopoulos, "On the effect of substrate thickness and permittivity and permittivity on printed circuit dipole performance," *IEEE Trans. Antennas Propagat.*, vol. AP-31, pp. 34–38, Jan. 1983.

[17] N. G. Alexopoulos, P. B. Katehi, and D. Rutledge, "Substrate optimization for integrated circuit applications," *IEEE Trans. Microwave Theory Tech.*, vol. MTT-31, pp. 550–557, July, 1983.

[18] P. B. Katehi and N. G. Alexopoulos, "Frequency-dependent characteristics of microstrip discontinuities in millimeter-wave integrated circuits," *IEEE Trans. Microwave Theory Tech.*, vol. MTT-33, pp. 1029–1035, Oct. 1985.

[19] R. W. Jackson and D. M. Pozar, "Full-wave analysis of microstrip open-end and gap discontinuities," *IEEE Trans. Microwave Theory Tech.*, vol. MTT-33, pp. 1036–1042, Oct. 1985.

[20] H. Yang, N. G. Alexopoulos, and D. R. Jackson, "Analysis of microstrip open-end and gap discontinuities in a substrate–superstrate configuration," *IEEE MTT-S Int. Microwave Symp. Dig.*, June 1988, pp. 705–708.

[21] R. Jackson, "Full-wave finite element analysis of irregular microstrip discontinuities," *IEEE Trans. Microwave Theory Tech.*, vol. 37, pp. 81–89, Jan. 1989.

[22] W. P. Harokopus, Jr., and P. B. Katehi, "An accurate characterization of open microstrip discontinuities including radiation losses," in *IEEE MTT-S Int. Microwave Symp. Dig.*, June 1989, pp. 231–234.

[23] N. K. Das and D. M. Pozar, "A generalized spectral-domain Green's function for multilayer dielectric substrates with application to multilayer transmission lines," *IEEE Trans. Microwave Theory Tech.*, vol. MTT-35, pp. 326–335, Mar. 1987.

[24] A. Sommerfeld, *Partial Differential Equations in Physics*. New York: Academic Press, 1949.

[25] R. S. Elliott, "The Green's function for electric dipoles parallel to and above or within a grounded dielectric slab," Hughes Technical Correspondence, 1978.

[26] R. F. Harrington, *Field Computation By Moment Methods*. New York: Macmillan, 1968.

[27] N. G. Alexopoulos and D. R. Jackson, "Fundamental superstrate (cover) effects on printed circuit antennas," *IEEE Trans. Antennas Propagat.*, vol. AP-32, pp. 807–814, Aug. 1984.

[28] W. Wertgen and R.H. Jansen, "Spectral iterative techniques for the full-wave 3-D analysis of (M)MIC structure," in *IEEE MTT-S Int. Microwave Symp. Dig.*, June 1988, pp. 709–712.

[29] P. B. Katehi and N. G. Alexopoulos, "Real axis integration of Sommerfeld integrals with applications to printed circuit antennas," *J. Math. Phys.*, vol. 24, no. 3, Mar. 1983.

William P. Harokopus, Jr. (S'87–M'87) was born in Detroit, MI, on February 10, 1963. He received the B.S. (1985) and M.S. (1986) degrees in electrical engineering from the University of Michigan, Ann Arbor. He is currently pursuing the Ph.D. degree at Michigan, where he works in the Radiation Lab as a graduate research assistant. His dissertation will be on the high-frequency characterization of microstrip discontinuities.

Pisti B. Katehi (S'81–M'84–SM'89) received the B.S.E.E. degree from the National Technical University of Athens, Greece, in 1977 and the M.S.E.E. and Ph.D. degrees from the University of California, Los Angeles, in 1981 and 1984 respectively.

In September 1984 she joined the faculty of the EECS Department of the University of Michigan, Ann Arbor, as an Assistant Professor. Since then, she has been involved in the modeling and computer-aided design of millimeter-wave and near-millimeter-wave monolithic circuits and antennas.

In 1984 Dr. Katehi received the W. P. King Award and in 1985 the S. A. Schelkunoff Award from the Antennas and Propagation Society. In 1987 she received an NSF Presidential Young Investigator Award and a Young Scientist Fellowship awarded from URSI. Dr. Katehi is a member of IEEE AP-S, MTT-S and Sigma Xi.